encit 2020

ABCM Associação Brasileira de Engenharia e Ciências Mecânicas

18th Brazilian Congress of Thermal Sciences and Engineering
November 16–20, 2020 (Online)

ENC-2020-0247
MEASUREMENT OF SPECTRAL EMISSIVITY IN METALS FOR LONG INFRARED WAVELENGTHS USING THERMAL IMAGERS

Matheus de Oliveira Moreira
Laboratório de Termometria - LabTerm, Programa de Pós-Graduação em Engenharia Mecânica, Escola de Engenharia, Universidade Federal de Minas Gerais, Belo Horizonte, MG, Brazil, 31270-901
Rafael A. M. Ferreira
Alexandre M. Abrão
Matheus P. Porto
Laboratório de Termometria - LabTerm e Departamento de Engenharia Mecânica, Escola de Engenharia, Universidade Federal de Minas Gerais, Belo Horizonte, MG, Brazil, 31270-901
matheusporto@ufmg.br

Abstract.
Emissivity is a physical property that relates temperature difference with heat transfer. Emissivity depends on a set of physical properties: molecule/surface temperatures, wavelength, directional dependence (optical properties, rugosity, etc.), and polarization. Spectral dependence in metallic surfaces can not be neglect, and gray body-based models may lead to inaccurate estimates of heat transfer and emissivity. The present study proposes a methodology to estimate long-wavelength spectral emissivity of metallic surfaces, using a thermal imager and mathematical models. We used a 7.5μm to 13μm infrared camera to measure the radiosity of an AISI H13 steel sample, at the same time as temperature was measured using a thermocouple type T. We upload the thermal images in Python, extract a matrix of radiosities, and post-process the experimental results using heat transfer relations and data from the literature, to estimate the spectral behavior of the metal surface. We tested temperatures from 50°C to 250°C, and spectral emissivity of AISI H13 steel ranged from 0.12 to 0.20. The results of spectral emissivity achieved with the proposed procedure were higher than those obtained by applying only theoretical models.

Keywords: *thermal radiation, spectral emissivity, longwave infrared, measurement, metal.*

1. INTRODUCTION

Surface emissivity is a function of several variables, such as the surface temperature, the direction of the emission, and the wavelength (Howell *et al.*, 2016). This property is essential for non-contact temperature measurements, but defining a surface emissivity value is not a simple task. As stated in Liu *et al.* (2013), it is often necessary to monitor the temperature of a steel surface during a manufacturing process using infrared-based devices in the industry. Due to the strong influence of the spectrum in the radiative properties of metals, the gray body hypothesis is hardly suitable for the radiative characterization of these types of surfaces (Vollmer and Möllmann, 2018). Mihalow (1988) also points out the roughness and surface impurities as variables of significant influence for the analysis of metallic surfaces. The author indicates that the emissivity of a steel surface can range from 0.1 to 0.9, and the wrong choice can jeopardize a measurement.

Theoretical models and experimental techniques are the options for predicting the emissivity value of a metallic surface (Howell *et al.*, 2016). Based on relations between the optical and the electrical properties of metals (Hagen and Rubens, 1900), scientific literature presents many expressions that describe the spectral behavior of the radiative properties (Howell *et al.*, 2016; Arata and Miyamoto, 1976; Bramson, 1968). The experimental techniques involve devices for measuring the target surface temperature and its radiosity. With those values, one can obtain the emissivity by comparing the infrared radiation from the target surface and the expected infrared radiation from a blackbody at the same temperature (Zhu *et al.*, 2020). Thermocouples are the most common instruments for the surface temperature measurement, while radiation thermometer (Zhu *et al.*, 2020), thermal imagers (Wang *et al.*, 2015; Valiorgue *et al.*, 2013; Li *et al.*, 2012), and spectrometers (Wang *et al.*, 2018; Wen, 2010; del Campo *et al.*, 2010) can measure the surface's radiosity.

The studies that used a thermal imager as the infrared based-device calculated the emissivity as a total value in the thermal imager spectral range of operation. Spectral emissivity usually demands the use of spectrometers. This study aims to propose a procedure to estimate spectral emissivity of metallic surfaces using a thermal imager. We combined the theoretical formulation presented by Hagen and Rubens (1900) and an experimental apparatus to estimate the spectral emissivity inside the thermal imager spectral range of operation. Our tests used AISI H13 steel as the specimen, and the

results achieved were analyzed and compared with the data presented in the scientific literature.

This article was divided into more four sections. Section 2 contains a description of a general infrared inspection using a thermal imager and the spectral emissivity mathematical formulations for metals. In section 3, we proposed a procedure for estimating the spectral emissivity of metallic surfaces using thermal imagers. Section 4 presents our results of spectral emissivity and the comparison with scientific and technical data. Our conclusions are presented in section 5.

2. INFRARED THERMOGRAPHY AND SPECTRAL EMISSIVITY

As presented by Minkina and Dudzik (2009), during a thermographic inspection, the signal received by the thermal imager's sensors comes from three different sources of infrared radiation: emission of the target surface, reflection of the radiation emitted by external bodies, and emission from the atmosphere between the thermal imager and the target surface. The thermal imager software calculates the surface temperature taking into account these three radiation sources. In order to calculate the surface temperature (T_{ob}), the user must input the following physical variables: total emissivity of the target surface (ε), reflected temperature (T_{ref}), atmospheric temperature (T_{atm}), ambient relative humidity ($\varphi_{\%}$), and distance between the thermal imager and the target surface (d).

Figure 1 shows a symbolic representation of a general situation of measurement using a thermography camera. The symbol τ_{atm} represents the transmissivity of the medium between the target surface and the thermal imager, and E refers to the blackbody's emissive power (Stefan-Boltzmann's Law).

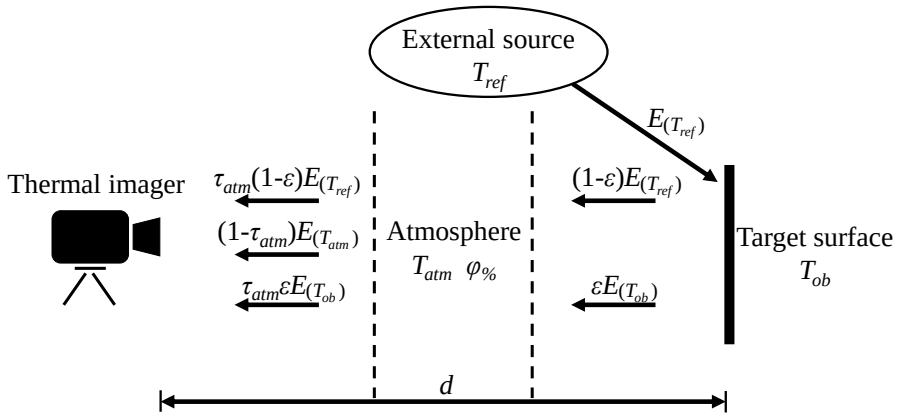

Figure 1: Radiative components of a thermography measurement.

Minkina and Daniel (2015) presented a formulation to calculate the transmissivity, for the longwave infrared band, of the ground level atmosphere using Eq. (1) and Eq. (2), where: T_{atm} should be converted from K to °C; K_{atm} = 1.9; α_1 = 0.066; α_2 = 0.0126; β_1 = -0.0023; β_2 = -0.0067; h_1 = 1.5587; h_2 = 6.939·10^{-2}; h_3 = -2.7816·10^{-4}; h_4 = 6.8455·10^{-7}.

$$\omega = \frac{\varphi_{\%}}{100} e^{\left(h_1 + h_2 T_{atm} + h_3 T_{atm}^2 + h_4 T_{atm}^3\right)} \tag{1}$$

$$\tau_{atm} = K_{atm} e^{\left[-\sqrt{d}\left(\alpha_1 + \beta_1\sqrt{\omega}\right)\right]} + \left(1 - K_{atm}\right) e^{\left[-\sqrt{d}\left(\alpha_2 + \beta_2\sqrt{\omega}\right)\right]} \tag{2}$$

Equation (3) is the mathematical statement that rules the calculation made by the thermal camera software (Tran *et al.*, 2017)

$$T_{ob} = \sqrt[4]{\frac{T_f^4 - (1-\varepsilon)\tau_{atm} T_{ref}^4 - (1-\tau_{atm}) T_{atm}^4}{\varepsilon \tau_{atm}}}, \tag{3}$$

where T_f is the apparent temperature and refers to the temperature value associated with the full signal received by the camera (full response), that is, the temperature value for a situation where the distance between the camera and the object is zero, and it is assumed a unitary emissivity surface. The formulation presented by Eq. (3) do not take into account the spectral behavior of the target surface radiative properties.

The surface emissivity refers to the energy that it radiates compared to the energy that a blackbody, under the same temperature, would be able to emit (Howell *et al.*, 2016). Emissivity is a function of at least three variables: spectrum; direction; temperature. Therefore, the emissivity may have directional-spectral behavior and temperature dependence. Analyzing a single direction, one can define the spectral emissivity according to Eq. (4)

$$\varepsilon_{(\lambda,T)} = \frac{I_{(\lambda,T)}}{I_{b(\lambda,T)}}, \tag{4}$$

where: λ refers to spectral dependence; T is the emitting surface absolute temperature; I is the spectral intensity of a real surface; I_b is the blackbody spectral intensity, given by Planck's Law (Eq. (5), where n is the refractive index, C_1 = $0.595522{\cdot}10^8 W\mu m^4 m^{-2} sr^{-1}$, and C_2 = $14387.77\mu mK$).

$$I_{b(\lambda,T)} = \frac{2C_1}{n^2\lambda^5\left[e^{\left(\frac{C_2}{n\lambda T}\right)}-1\right]} \tag{5}$$

Some correlations describe the theoretical behavior of the radiative properties of metals. From the electromagnetic wave theory, Hering and Smith (1968) proposed Eq. (6) and Eq. (7) to estimate the specular reflectivity (ρ) of an absorbing medium of large extinction coefficient (k) from its optical properties and the direction (θ). If the material has a thickness that ensures an opaque behavior, Eq. (8) and Eq. (9) determine the spectral-directional emissivity for parallelly and perpendicularly polarized radiation, respectively.

$$\rho_{\parallel(\lambda,\theta)} = \frac{\left(n_{(\lambda)}cos\theta - 1\right)^2 + \left(k_{(\lambda)}cos\theta\right)^2}{\left(n_{(\lambda)}cos\theta + 1\right)^2 + \left(k_{(\lambda)}cos\theta\right)^2} \tag{6}$$

$$\rho_{\perp(\lambda,\theta)} = \frac{\left(n_{(\lambda)} - cos\theta\right)^2 + k_{(\lambda)}^2}{\left(n_{(\lambda)} + cos\theta\right)^2 + k_{(\lambda)}^2} \tag{7}$$

$$\varepsilon_{\parallel(\lambda,\theta)} = 1 - \rho_{\parallel(\lambda,\theta)} \tag{8}$$

$$\varepsilon_{\perp(\lambda,\theta)} = 1 - \rho_{\perp(\lambda,\theta)} \tag{9}$$

Hagen and Rubens (1900) proposed a useful formulation to the prediction of the spectral emissivity of an optically smooth metallic surface for $\lambda > 5\mu m$. The Hagen-Rubens expression, Eq. (10), correlates the electrical resistivity (r_e) of metallic materials with their refractive index and extinction coefficient.

$$n_{(\lambda)} = k_{(\lambda)} = \sqrt{\frac{0.003\lambda}{r_e}} \tag{10}$$

Based on the Hering and Smith (1968) formulation for high extinction coefficient media (suitable for metals) and the Hagen-Rubens relation, it is possible to obtain equations that calculate spectral-directional emissivity from the electrical properties (Howell *et al.*, 2016). Equations (11), (12), and (13) show, respectively, the spectral-directional emissivity for parallelly polarized radiation, the spectral-directional emissivity for perpendicularly polarized radiation, and the relationship to obtain the spectral-directional emissivity for non-polarized radiation from the polarized ones.

$$\varepsilon_{\parallel(\lambda,\theta)} = \frac{4\sqrt{\frac{0.003\lambda}{r_e}}cos\theta}{\frac{0.006\lambda}{r_e}cos^2\theta + 2\sqrt{\frac{0.003\lambda}{r_e}}cos\theta + 1} \tag{11}$$

$$\varepsilon_{\perp(\lambda,\theta)} = \frac{4\sqrt{\frac{0.003\lambda}{r_e}}cos\theta}{cos^2\theta + 2\sqrt{\frac{0.003\lambda}{r_e}}cos\theta + \frac{0.006\lambda}{r_e}} \tag{12}$$

$$\varepsilon_{(\lambda,\theta)} = \frac{\varepsilon_{\parallel(\lambda,\theta)} + \varepsilon_{\perp(\lambda,\theta)}}{2} \tag{13}$$

Temperature affects the electrical resistivity of metals. This dependence is represented by the temperature coefficient of resistivity (γ) (Kasap, 2018). Equation (14) shows the mathematical expression to obtain the electrical resistivity from the temperature coefficient and a reference pair of electrical resistivity (r_{e_0}) and temperature (T_0). Equation (15) demonstrates the temperature dependence of γ, where γ_0 is the reference value of temperature coefficient of resistivity.

$$r_{e(T)} = r_{e_0}e^{[\gamma(T-T_0)]} \tag{14}$$

$$\gamma_{(T)} = \frac{1}{\frac{1}{\gamma_0} + (T - T_0)} \tag{15}$$

3. METHODS

The methodology applied to the present study is divided into two parts: experimental tests and mathematical model.

3.1 Experimental tests

Our experiments were based on infrared inspections of a sample of AISI H13 steel, a high alloy tool steel. Table 1 shows the sample chemical composition in weight percent ($wt\%$) and the ASTM requirements for the AISI H13 steel. The steel sample had a parallelepiped shape (105mm x 20mm x 16mm), with one of its faces finished by face milling and with a 3mm diameter and 8mm deep hole produced by drilling. We measured the surface roughness using a Taylor Hobson Surtronic 25 roughness meter and obtained the arithmetical mean deviation of the roughness profile (R_a parameter) equals to $0.37\mu m$.

Table 1: AISI H13 steel chemical composition ($wt\%$).

	C	Mn	Si	Cr	V	Mo	Fe
Sample	0.35	0.31	0.95	4.89	0.85	1.17	Balance
ASTM A681	0.32 - 0.45	0.20 - 0.60	0.80 - 1.25	4.75 - 5.50	0.80 - 1.20	1.10 - 1.75	Balance

We carried out the tests with controlled ambient conditions: ambient temperature between 20°C and 24°C, and relative humidity between 45% and 70%. A digital thermo-hygrometer, model Testo 622, was used for monitoring the ambient conditions. The thermal imager used in the infrared inspections was the Flir SC660 thermal camera with a 19mm focal length lens, equipment that operates in the longwave infrared (LWIR) band of the spectrum ($7.5\mu m$ to $13\mu m$), and that has a resolution of 640 x 480 pixels. Simultaneously with the thermographic tests, the temperature of the specimen was measured using a type T thermocouple, and the data acquisition system NI 9211 Series C.

The metallic sample was carefully manipulated in order to avoid any superficial damage and its surface was cleaned using ethanol and acetone to remove the superficial impurities. After the initial preparation, the steel sample was heated in a muffle furnace until it reached the temperature required. Then, it was removed from the furnace and taken to an MDF box thermally insulated by rock wool. The face with surface finishing by milling of the sample was left upward. At this point, the thermocouple was placed in the drilled hole of the sample and the test effectively begins. The thermal imager, programmed to measure the apparent temperature (ε = 1 and d = 0), captured thermograms of the sample metal surface at a frequency of 1Hz and, simultaneously, the surface temperature was measured with the type T thermocouple and the data acquisition system at the rate of 10Hz.

Figure 2 shows a symbolic representation of the test arrangement. The thermal imager was positioned at an angle (θ) of 37° relative to the normal line to the surface of the sample, keeping a distance of 240mm from this surface. The test was repeated for eight different surface temperatures from 50°C to 250°C.

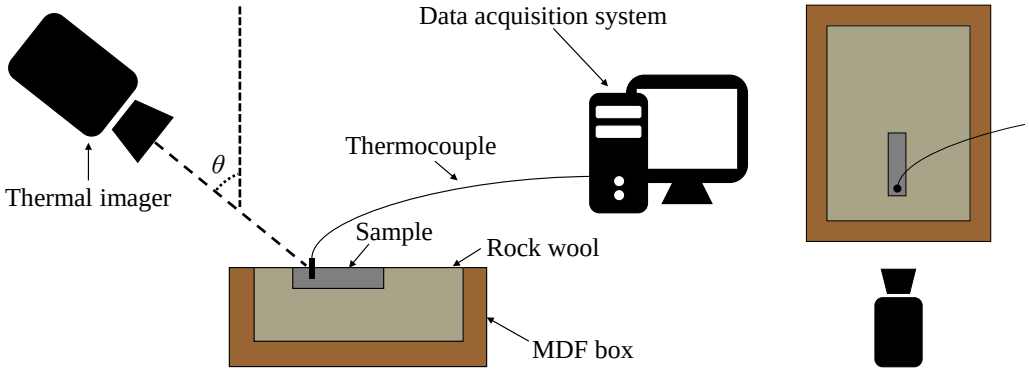

(a) Side view. (b) Upper view.

Figure 2: Experimental apparatus for the emissivity estimation.

3.2 Mathematical model

From Eq. (11), Eq. (12), and Eq. (13), one can obtain the spectral behavior of emissivity from the electrical resistivity, the wavelength, and the direction. In our study, the electrical resistivity was initially unknown. We propose a mathematical model to obtain the electrical resistivity and the spectral emissivity of a metallic sample as a function of its temperature. However, as the electrical resistivity is an input variable to the Hagen-Rubens equation, it was necessary to use an iterative calculation routine.

Applying the spectral radiation model presented by Ferreira *et al.* (2019) to our experimental approach, we calculated the three spectral radiation components received by the thermal imager sensors using the Eq. (16), Eq. (17), Eq. (18)

$$S_{ob(\lambda)} = \varsigma_{(T_{ob})} S_{k(\lambda)} \tau_{atm} \varepsilon_{(\lambda,T_{ob})} I_{b(\lambda,T_{ob})} \tag{16}$$

$$S_{ref(\lambda)} = \varsigma_{(T_{ref})} S_{k(\lambda)} \tau_{atm} \rho_{(\lambda,T_{ob})} I_{b(\lambda,T_{ref})} \tag{17}$$

$$S_{atm(\lambda)} = \varsigma_{(T_{atm})} S_{k(\lambda)} \left(1 - \tau_{atm}\right) I_{b(\lambda,T_{atm})} \tag{18}$$

where: S_{ob} is the signal related to the radiation emitted by the target; S_{ref} is the signal related to the radiation reflected by the target; S_{atm} is the signal related to the radiation emitted by the ground level atmosphere; S_k is the thermal imager relative spectral sensitivity; ς is a function that converts the radiometric signal ($Wm^{-2}sr^{-1}\mu m^{-1}$) into the response signal; ρ is the spectral reflectivity of the target, which we calculate from the spectral emissivity, assuming the opaque surface hypothesis, Kirchhoff's Law, and a single direction.

The thermal imager full response gives the full signal (S_f), as presented in Eq. (19).

$$S_{f(\lambda)} = \varsigma_{(T_f)} S_{k(\lambda)} I_{b(\lambda,T_f)} \tag{19}$$

The remaining unknown variable was the electrical resistivity. In order to calculate it, we implemented an iterative routine using the balance of the inputs and output signals in the thermal imager. The numerical integration of the sum of the inputs signals (S_{in}) and the full signal over the LWIR must be equal. Equations (20) and (21) illustrate the signal balance, where the admissible deviation was set as 0.01% of the total full signal.

$$S_{in(\lambda)} = S_{ob(\lambda)} + S_{ref(\lambda)} + S_{atm(\lambda)} \tag{20}$$

$$\sum_{7.5\mu m}^{13\mu m} \left(S_{f(\lambda)} \Delta\lambda\right) - \sum_{7.5\mu m}^{13\mu m} \left(S_{in(\lambda)} \Delta\lambda\right) < 0.01\% \sum_{7.5\mu m}^{13\mu m} \left(S_{f(\lambda)} \Delta\lambda\right) \tag{21}$$

It was necessary to input an initial guess for the electrical resistivity to solve the iterative routine proposed. The outputs of this routine were the electrical resistivity value, which made the routine converge, and the respective values of spectral emissivity. Both values were related to the object temperature, one of the experimental inputs. The other inputs were the ambient conditions (temperature and relative humidity), the apparent temperature, the direction, and the spectral range of the thermal imager. Using Python, we got the apparent temperature from the thermograms of the infrared inspections.

4. RESULTS AND DISCUSSION

We estimated the spectral emissivity of the AISI H13 steel sample for eight different temperatures in the range of 50°C to 250°C. The estimation was based on the thermal imager signals balance. Our results are composed of spectral emissivity estimates and the analysis of the thermal imager signals.

4.1 Spectral emissivity

The temperatures used for the spectral emissivity calibration were: 67°C, 121°C, 132°C, 139°C, 162°C, 192°C, 221°C, and 242°C. Figure 3 shows the results of spectral emissivity and electrical resistivity. The electrical resistivity results are compared with those obtained from the equation presented by Rosales-Saiz *et al.* (2016). The values of spectral emissivity and electrical resistivity tended to increase with temperature.

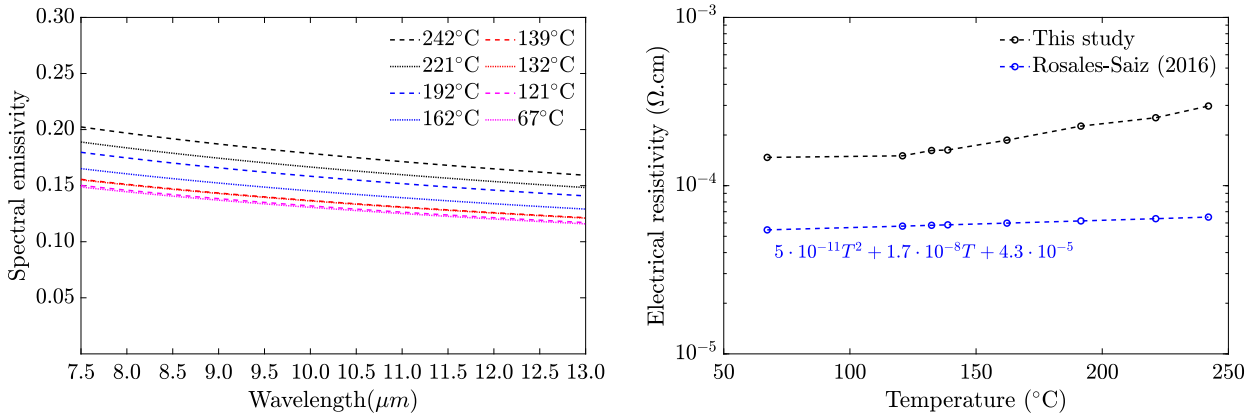

(a) Spectral emissivity.

(b) Electrical resistivity.

Figure 3: Results for the AISI H13 steel sample.

The electrical resistivity of the AISI H13 steel sample presented values higher than those predicted using the Rosales-Saiz formulation. The temperature dependence in the experimental results was more intense than in the theoretical values.

According to the Hagen-Rubens equation, the spectral emissivity of metals is proportional to the electrical resistivity square root. So, the upward temperature behavior of the spectral emissivity was due to the temperature dependence exhibited by the electrical resistivity (Fig. 3).

Our spectral emissivity results were complementary to those presented by Wen (2010). The author measured the spectral emissivity of AISI H13 steel in the wavelength range of $2.8\mu m$ to $4.2\mu m$ for the temperature values of 427°C, 527°C, and 627°C. Figure 4 illustrates the results from Wen (2010) and this study. Each box contains the spectral emissivity estimates for an AISI H13 sample at a different temperature. Higher emissivity values are related to lower wavelengths (in the work spectral range of each study), following the trend presented in Fig. 3.

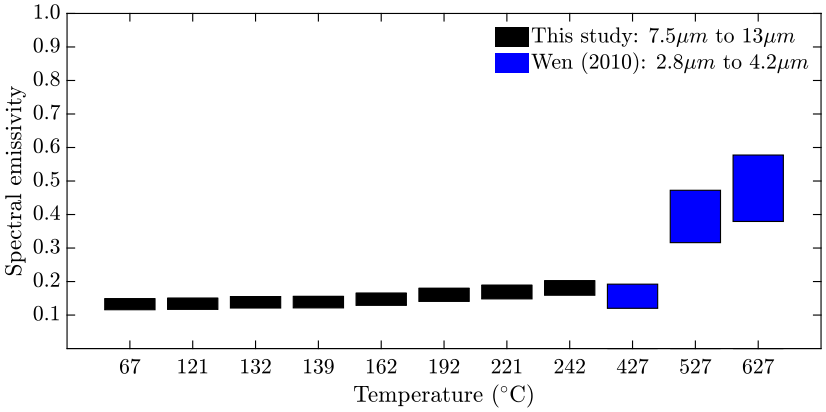

Figure 4: AISI H13 steel emissivity values for different spectral ranges and temperatures.

Arata and Miyamoto (1976) and Bramson (1968) proposed equations that can be used to theoretical estimation of the spectral emissivity of metals. Figure 5 presents the temperature effect on spectral emissivity for the wavelength of $10.6\mu m$ of AISI H13 steel. The results based on Arata-Miyamoto and Bramson formulations used the electrical resistivity values of Rosales-Saiz *et al.* (2016). The theoretical values of spectral emissivity were lower than our results. This difference increased when the temperature rose. The use of the theoretical emissivity results can lead to higher temperatures during measurement using an infrared-based device. This type of instrument usually demands an emissivity calibration process before the measurement in order to minimize the errors in the results.

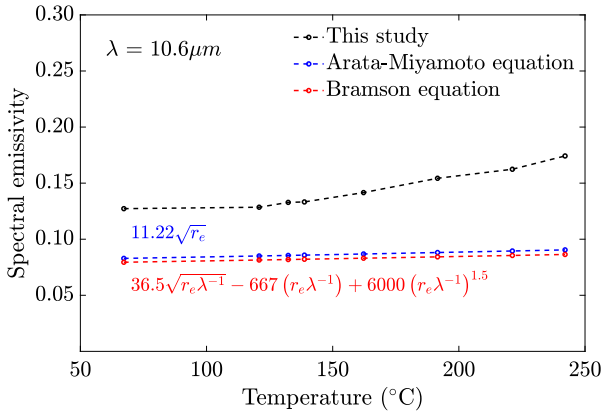

Figure 5: Experimental and theoretical values of spectral emissivity for the wavelength of $10.6\mu m$.

Although our study aimed to estimate the spectral emissivity of the AISI H13 steel sample in the range of 50°C to 250°C, we calculated the spectral emissivity for ambient temperature (300K) in order to compare to the steel emissivity data presented by scientific and technical literature. To do that, we extrapolated our values of electrical resistivity, following the relation presented by Eq. (14) and Eq. (15). Figure 6 shows the extrapolated results with the spectral emissivity data from Berkmanns and Faerber (2010) and Ready (1997) for steel. The values of spectral emissivity obtained using the proposed procedure presented good agreement with the scientific and technical literature.

4.2 Thermal imager signals

We used numerical integration to calculate the total signal, over the long infrared wavelength band, for each source of radiation. Figure 7 illustrates the ratio of the integration of each infrared component (S_{ob}, S_{ref}, and S_{atm}) and the integration of the full signal (S_f). This ratio informs which infrared source dominates the thermal imager full response.

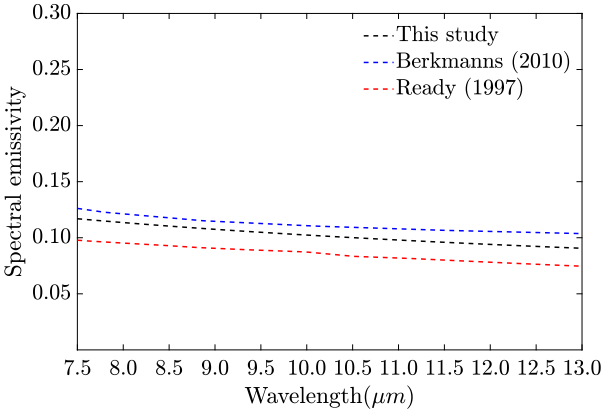

Figure 6: Spectral emissivity for ambient temperature.

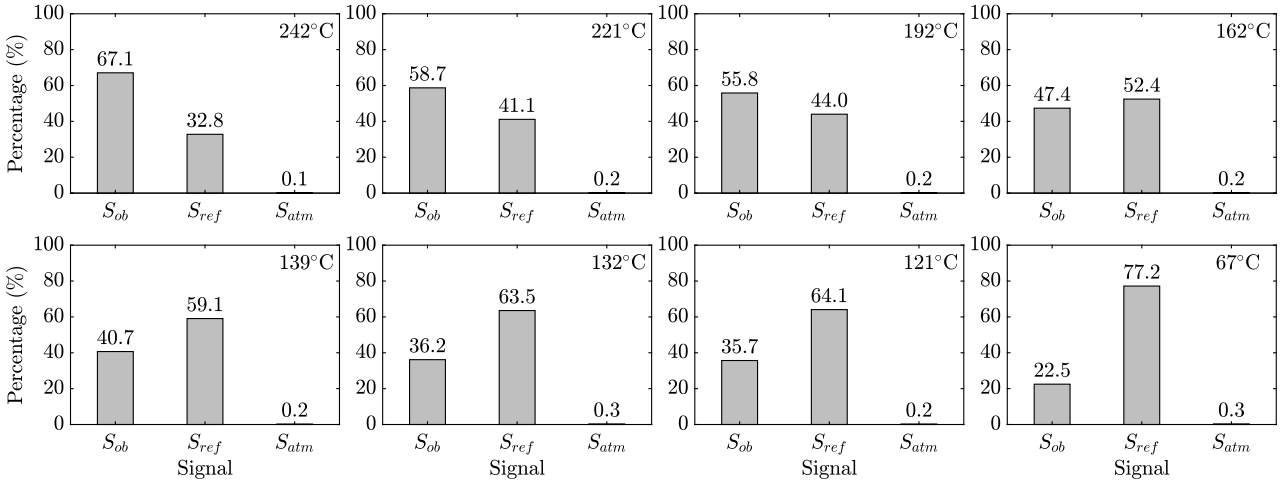

Figure 7: Distribution of full signal among the inputs S_{ob}, S_{ref}, and S_{atm}.

Figure 7 shows that for higher temperatures, the radiation emitted by the target has the main influence on the full signal, while the reflected radiation plays this role for lower temperatures. This behavior is explained by the temperature influence in the spectral emissivity. The higher the temperature, the higher the spectral emissivity and the lower the spectral reflectivity (according to the opaque surface hypothesis). With higher values of emissivity and lower values of reflectivity, the surface emits more infrared radiation, while reflects less intensely the incident radiation that was emitted by the surroundings. Thus, the characterization of external sources of heat before the emissivity calibration is even more critical for low target temperature situations. Infrared measurements should be performed under controlled ambient conditions when possible. The atmosphere emission contribution was approximately zero in the eight experiments. Hence, if the conditions of measurement (equipment, distance, ambient temperature, and relative humidity) are approximately those used in our experimental tests, the S_{atm} might be neglected to simplify the calculation.

5. CONCLUSION

This study presented a procedure for estimating the spectral emissivity of metals using longwave infrared thermal imagers. The procedure involved an experimental approach and a mathematical post-processing routine. For the experimental part, we used a thermal imager that operates in the long infrared wavelength and a type T thermocouple connected to a data acquisition system to measure the surface radiosity and temperature, respectively. A sample of AISI H13 steel with the upside surface finished by milling was the target object. We repeated the experiment for eight different sample temperatures in the range of 50°C to 250°C. The post-processing routine used the Hagen-Rubens relation associated with a spectral radiation heat transfer formulation.

The results achieved with the proposed procedure showed that the AISI H13 steel spectral emissivity tended to increase with temperature. Spectral emissivity values ranged from 0.12 to 0.20, increasing with temperature and reducing with wavelength. The same tendency was found for electrical resistivity results, as expected for metals. However, the values of spectral emissivity and electrical resistivity were higher than those predicted by theoretical models. The temperature effect was also more intense in the results obtained using the proposed procedure.

We integrated the spectral signals over the thermal imager spectral range (7.5μm to 13μm). This study showed that

the infrared radiation emitted by external sources of heat and reflected by the AISI H13 steel played an important role when the sample temperature was lower. So, it is important to perform the infrared measurement in controlled conditions when possible. We found that the atmosphere longwave infrared emission contribution for the thermal imager output signal is negligible if the conditions of measurement are similar to those used in this work.

6. ACKNOWLEDGEMENTS

This is study was financed in part by the Conselho Nacional de Desenvolvimento Científico e Tecnológico - Brazil (CNPq), by the Coordenação de Aperfeiçoamento de Pessoal de Nível Superior - Brazil (CAPES), and by the PRPq-UFMG (Pró-Reitoria de Pesquisa da Universidade Federal de Minas Gerais).

7. REFERENCES

Arata, Y. and Miyamoto, I., 1976. "Laser Welding". *Technocrat*, Vol. 11, No. 5, pp. 33–42.

ASTM A681, 2007. "Standard Specification for Tool Steels Alloy". Standard, ASTM International, West Conshohocken, PA.

Berkmanns, J. and Faerber, M., 2010. "Laser basics. LASERLINE® Technical". Technical documentation, BOC Group.

Bramson, M., 1968. *Infrared Radiation: A Handbook for Applications*. Plenum Press.

del Campo, L., Pérez-Sáez, R., González-Fernández, L., Esquisabel, X., Fernández, I., González-Martín, P. and Tello, M., 2010. "Emissivity measurements on aeronautical alloys". *Journal of Alloys and Compounds*, Vol. 489, No. 2, pp. 482–487.

Ferreira, R.A.M., Pottie, D.L.F., Dias, L.H.C., Cardoso Filho, B.J. and Porto, M.P., 2019. "A directional-spectral approach to estimate temperature of outdoor PV panels". *Solar Energy*, Vol. 183, pp. 782–790.

Hagen, E. and Rubens, H., 1900. "Metallic reflection". *Ans. Phys.*, Vol. 1, No. 2, pp. 352–375.

Hering, R. and Smith, T., 1968. "Surface radiation properties from electromagnetic theory". *International Journal of Heat and Mass Transfer*, Vol. 11, No. 10, pp. 1567 – 1571.

Howell, J.R., Mengüç, M.P. and Siegel, R., 2016. *Thermal Radiation Heat Transfer*. CRC Press, Boca Raton, 6th edition.

Kasap, S.O., 2018. *Electrical and Thermal Conduction in Solids*, McGraw-Hill, chapter 2, pp. 125–212. 4th edition.

Li, H.Q., Zhang, Y.S., Wang, L., Tian, X.W., Wang, C. and Zhu, B., 2012. "Emissivity Calibration and Temperature Measurement of High Strength Steel Sheet in Hot Stamping Process". In *Applied mechanics and materials*. Trans Tech Publ, Vol. 148-149, pp. 1473–1477.

Liu, Y.F., Hu, Z.L., Shi, D.H. and Yu, K., 2013. "Experimental Investigation of Emissivity of Steel". *International Journal of Thermophysics*, Vol. 34, No. 3, pp. 496–506.

Mihalow, F.A., 1988. "Radiation Thermometry in the Steel Industry". In D.P. DeWitt and G.D. Nutter, eds., *Theory and Practice of Radiation Thermometry*, John Wiley Sons, chapter 16, pp. 861–904.

Minkina, W. and Daniel, K., 2015. "Modeling of atmospheric transmission coefficient in infrared for thermovision measurements". In *14th International Conference on Infrared Sensors Systems*. pp. 903–907.

Minkina, W. and Dudzik, S., 2009. *Infrared Thermography: Errors and Uncertainties*. John Wiley and Sons, Chippenham, 1st edition.

Ready, J., 1997. *Industrial Applications of Lasers*. Academic Press, San Diego, 2nd edition.

Rosales-Saiz, F., Pérez-Acosta, L., Machado, I.F., Pérez-Fernández, J.E., Jardim, R.F. and Govea-Alcaide, E., 2016. "Influence of spark plasma consolidation conditions on the superconducting properties of (Bi,Pb)-Sr-Ca-Cu-O ceramic samples". *Ceramics International*, Vol. 42, No. 15, pp. 17482 – 17488.

Tran, Q.H., Han, D., Kang, C., Haldar, A. and Huh, J., 2017. "Effects of Ambient Temperature and Relative Humidity on Subsurface Defect Detection in Concrete Structures by Active Thermal Imaging". *Sensors*, Vol. 17, No. 8, pp. 1718–1735.

Valiorgue, F., Brosse, A., Naisson, P., Rech, J., Hamdi, H. and Bergheau, J.M., 2013. "Emissivity calibration for temperatures measurement using thermography in the context of machining". *Applied Thermal Engineering*, Vol. 58, No. 1-2, pp. 321–326.

Vollmer, M. and Möllmann, K.P., 2018. *Infrared Thermal Imaging: Fundamentals, Research and Applications*. Wiley-VCH, Weinheim, 2nd edition.

Wang, P., Hu, Z., Xie, Z. and Yan, M., 2018. "A new experimental apparatus for emissivity measurements of steel and the application of multi-wavelength thermometry to continuous casting billets". *Review of Scientific Instruments*, Vol. 89, No. 5, p. 054903.

Wang, P., Xie, Z., Meng, H. and Hu, Z., 2015. "Effects of the temperature and roughness on the metal emissivity". In *27th Chinese Control and Decision Conference (2015 CCDC)*. IEEE, pp. 6197–6200.

Wen, C.D., 2010. "Investigation of steel emissivity behaviors: Examination of Multispectral Radiation Thermometry (MRT) emissivity models". *International Journal of Heat and Mass Transfer*, Vol. 53, No. 9-10, pp. 2035–2043.

Zhu, C., Hobbs, M.J. and Willmott, J.R., 2020. "An accurate instrument for emissivity measurements by direct and

indirect methods". *Measurement Science and Technology*, Vol. 31, No. 4, p. 044007.

8. RESPONSIBILITY NOTICE

The authors are solely responsible for the printed material included in this paper.